The Detection and Classification of Radio Frequency Interference in the Soil Moisture Active Passive Dataset

Thesis

Presented in Partial Fulfillment of the Requirements for Honors Research Distinction in Electrical and Computer Engineering at The Ohio State University

By

Anna Bete

Undergraduate Program in Computer Science and Engineering

The Ohio State University

2023

Thesis Committee

Dr. Alexandra Bringer, Advisor

Professor Joel Johnson, Advisor

Professor Bob Burkholder, Committee Member

Abstract

Soil moisture data is used in weather forecasting, drought detection, flood anticipation, and crop monitoring. NASA's Soil Moisture Active Passive (SMAP) mission orbits the Earth and operates a L-Band radiometer measuring the natural emission from the Earth to retrieve soil moisture. Despite the L-Band being a protected part of the spectrum to allow for passive observation of the Earth, radio frequency interferences (RFI) are observed in the SMAP measurements. This RFI is generated by illegal emissions within the protected band or by transmitters in adjacent frequency bands. Detecting RFI is critical, as it corrupts the radiometer measurements and can potentially bias the soil moisture retrievals, if the RFI is undetected. The detection is possible thanks to nine detection algorithms that are implemented in ground processing. Despite the overall good performance of the detection algorithms, some undetected RFI, also defined as residual RFI, are still noticeable in the SMAP measurements. This research is divided into two parts. The first part of the work focuses on classifying RFI sources using deep learning to provide a better understanding of the RFI environment. In this part of this study, the brightness temperatures for each SMAP radiometer measurement, or footprint, are treated as an image which will be the input to a deep learning neural network to classify the types of RFI into three groups: no RFI, wideband RFI, and narrowband RFI. The first results confirmed that using a neural network to classify different RFI types is possible and the SMAP footprints were

successfully classified with and accuracy of 98%. The second part of the project investigates the implementation of image processing techniques to detect residual RFI by using mean filtering to detect and remove residual RFI in SMAP data. The filter was used on weekly max hold filtered brightness temperature maps, i.e., after RFI detection was performed and convolves over the global image, identifying regions with large spatial variations. Initial results for the mean filtering algorithm demonstrated the potential of this technique to detect spatial areas contaminated with residual RFI sources.

Dedication

To my parents and Peter, for their never-ending encouragement.

To Alexandra, for helping me every step of the way.

Acknowledgments

I would first like to thank Dr. Alexandra Bringer for allowing me to work on this project and for giving me so much creative freedom in determining how to develop the solution, for educating me in the history of SMAP, and for providing weekly guidance. Without her help, I would not have been able to apply for undergraduate research distinction and receive a scholarship, present at the Denman Research Forum, or write and defend my thesis. I would also like to thank Dr. Joel Johnson for introducing me to this project, providing me with computer resources, and for his continued support and guidance. Thank you to Dr. Alexandra Bringer, Dr. Joel Johnson, and Dr. Bob Burkholder for serving on my defense committee.

Vita

2019 ……..……Carroll High School

2023 ……. B.S. Computer Science and Engineering, The Ohio State University

Funding

2021 …… Undergraduate Research Scholarship

Fields of Study

Major Field: Computer Science and Engineering

Table of Contents

List of Tables

List of Figures

Introduction

SMAP Background

On January 31, 2015, the National Aeronautics and Space Administration (NASA) launched their Soil Moisture Active Passive (SMAP) mission, which collects global soil moisture measurements for use in weather forecasting, drought detection, flood anticipation, crop monitoring, and water, energy, and carbon cycle tracking [1].

SMAP operates a L-Band radiometer in the 1400-1427 MHz range, a protected part of the electromagnetic spectrum to allow for passive observations of the Earth. Despite measuring in the protected range, the SMAP dataset is frequently corrupted by RFI and contains high levels of RFI in some locations [2].

The SMAP digital backend was specially designed to be able to perform RFI detection and filtering. More than eight years of RFI data are now available and can be used to infer information about the RFI environment. Previous studies analyzed maps and their time variations to obtain insight about the changes of the RFI environment, but those analyses don't provide information on the RFI sources directly (i.e., source types or the frequency most flagged). Given the large quantity of RFI data available, machine learning algorithms can be used to classify RFI sources to provide more information about the RFI sources. The first part of this research project focused on developing convolutional neuronal networks (CNN) to perform a classification of SMAP subband spectrograms into

three classes (no RFI, narrowband, wideband). This classification can be used to provide additional details about the RFI sources contained in each SMAP footprint. The accuracy of the classification using two CNNs will be presented in the first part of this thesis.

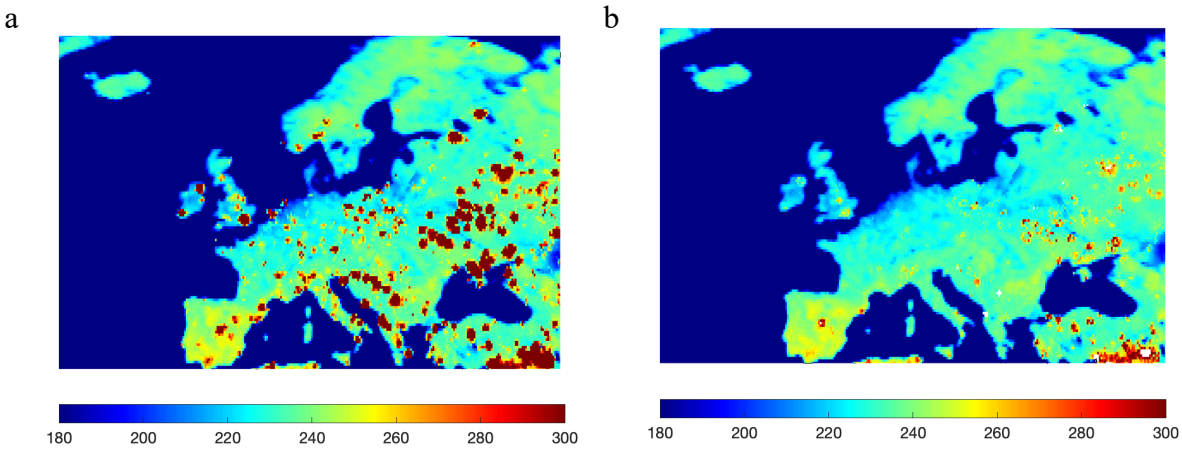

Figure 1: Max hold maps of SMAP Antenna Temperatures in vertical polarization a) before RFI detection algorithms are applied b) after RFI detection algorithms are applied for the week of 02/27/23.

Figure 1 presents an example of max hold maps of the SMAP antenna temperature in vertical polarization over Europe for the week of 02/27/2023 before RFI detection algorithms are applied (Figure 1a) and after RFI detection is performed (Figure 1b). The RFI sources appear as “hotter” spots in the Figure and a lot of them are identified and filtered by the SMAP algorithms, as shown on Figure 1b. However, despite the good performance of these algorithms to filer the RFI sources [3], some RFI sources can still be noticed in the max hold maps of the filtered antenna temperature (Figure 1b). This indicates that some RFI are undetected and remain in the data even after the RFI detection and filtering are applied. Those residual RFI are a concern as they could potentially induce bias in the soil moisture retrievals. Finding techniques to identify those residual RFI is a critical

topic that this research investigates using basic image processing to identify spatial areas impacted by RFI. Preliminary results will be presented in the second part of this thesis.

Related Work

SMAP is the first radiometer that provides information about RFI sources due to the design of its digital backend. Given the large amount of RFI data available, machine learning algorithms can be applied to SMAP spectrograms to do classification. Mohammed and Piepmeier [4] were the first to use a deep learning algorithm to detect the presence of RFI in SMAP spectrograms. In this case, deep learning was implemented by using a neural network to classify the output.

Computer vision neural networks, that is, networks that use images for their input, are composed of many layers – the first layers have functions such as identifying edges and colors on the image, while the final layers are project specific and classify the output. Transfer learning is the practice of replacing these final, project-specific layers to train the neural network to solve a new problem. Mohammed and Piepmeier used transfer learning to classify SMAP spectrograms into two groups: "RFI" and "No RFI" to identify the presence of RFI in the footprints. Their results are presented in [4] and they demonstrated that machine learning algorithms using CNNs could identify RFI in SMAP footprints with an accuracy of over 96% for each of the three CNNs tested.

Since they demonstrated the potential of using machine learning algorithms for separating SMAP footprints into RFI free footprints and RFI corrupted footprints, this work furthers their research by refining the classification to provide more characteristics about

the RFI sources. In this study, the use of machine learning algorithms using CNNs is investigated to classify the SMAP footprints into three classes: narrowband RFI, wideband RFI and no RFI.

The second part examines the issue of residual RFI and investigates new techniques to detect areas impacted these residual RFI. Previous studies were performed to investigate why the SMAP RFI algorithms failed to detect those RFI. Bringer et al. [5] studied several cases of residual RFI and showed, that in most cases, the residual RFI were moderate wideband continuous RFI. The SMAP algorithms were mainly designed to look for rapid changes in the antenna temperatures over time or frequency; therefore, they fail at detecting moderate wideband continuous RFI. Soldo et al [6] proposed an algorithm to identify spatial outlier in the antenna temperature measurements after RFI detection was applied for each SMAP half orbits. This spatial algorithm was based on contouring the antenna temperatures with iso lines and identify region with large gradients. In [6], Soldo et al, showed successful identification of residual RFIs. The second part of this work aims at using image processing algorithms to detect residual RFI on the weekly max hold maps of the filtered antenna temperature measurements, i.e., after RFI detection is applied, and potentially filter the residual RFIs. The first step of this work was to investigate the use of mean filtering to test the methodology before implementing the machine learning algorithm.

RFI Type Classification Initial Testing

Materials and Methods

The goal if this work is to classify the RFI sources to get more knowledge about the RFI environment. Previous studies [2] demonstrated the potential of using deep learning to identify the presence of RFI in SMAP footprints. This research expands upon their work by further classifying SMAP footprints that contains RFI into two different classes: narrowband and wideband. To do so, the SMAP footprints of the subband product, also referred to as spectrograms, were used as input to a deep learning neural network. The spectrograms represent the brightness temperature measurements for each of the 16 sub-frequency channels in eight sub-intervals of time. The spectrograms were treated as images by the neural network and frequency characteristics of the RFI were used to define the two additional classes. Therefore, the SMAP footprints will finally be classified into three groups: no RFI, wideband RFI, and narrowband RFI by the neural network. There is no set metrics for defining narrowband and wideband RFI. However, after a first examination of a significant number of SMAP footprints, it was chosen to define the narrowband RFI as RFI contaminating four or fewer frequency sub-channels and wideband RFI as RFI that impacted more than five frequency channels. Example footprints for each class are shown in Figure 2.

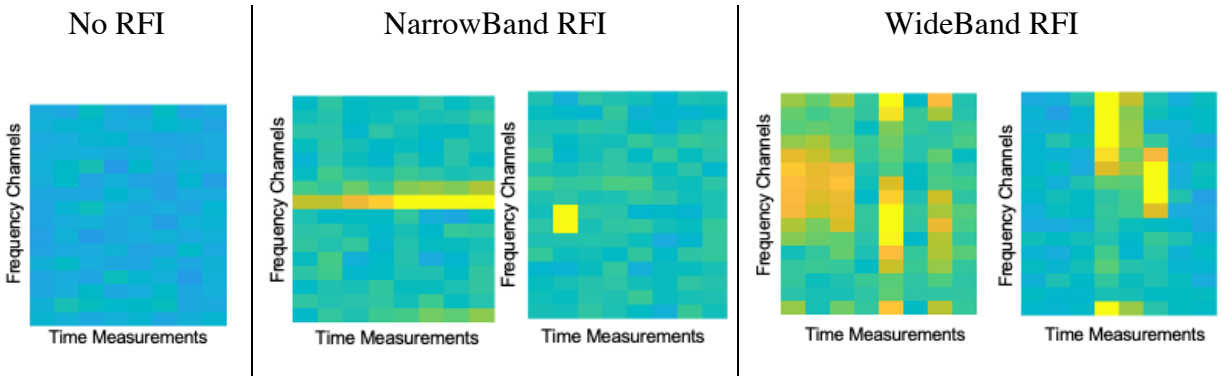

Figure 2: Example of SMAP footprints for each class.

Neural Network Setup.

Transfer learning is the process of using an existing neural network for a new purpose. Figure 3 shows a general outline of how a network is used in transfer learning. The first step consists in loading a pretrained network. Since these pretrained networks use images as their input, most of the network layers can keep their weights from their original training, since many of those layers are used to identify simple image characteristics such as edges, shapes, and color. The final layers of the network focus on classification and need to be replaced so that they will be trained for the new situation.

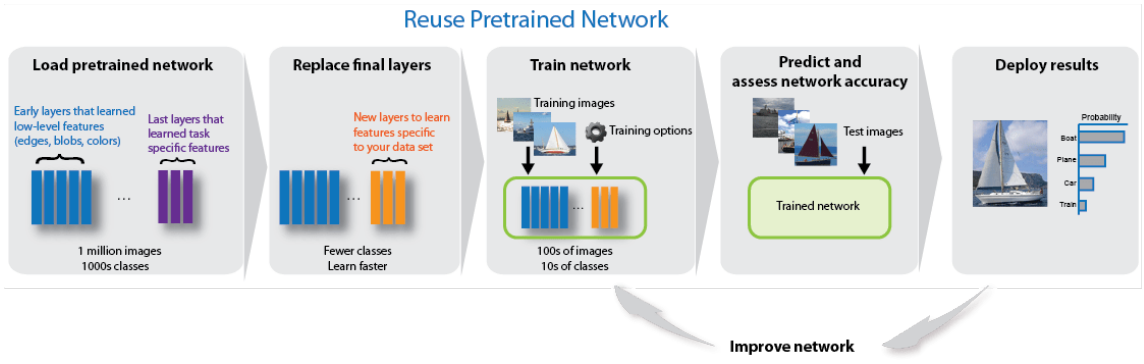

Figure 3: The transfer learning process [7].

In this work, transfer learning was chosen to be used as it is fast to setup, can require fewer images to train on, and works well for classification. Neural networks are usually evaluated on their accuracy, speed, and size, as presented in Figure 4. For this study, two neural networks, AlexNet and Resnet-101, are chosen and their performance in terms of classification accuracy will be compared. AlexNet has a lower accuracy, but it is faster to train. Resnet-101 presents a good compromise between accuracy and training time. Since AlexNet has a faster training time, it is easier to first determine the training parameters, such as learning rate and number of epochs to train, that are optimal for the training set. The parameters optimized for AlexNet serve as a starting point to find ResNet-101 parameters and will be tweaked to optimize the accuracy of the classification.

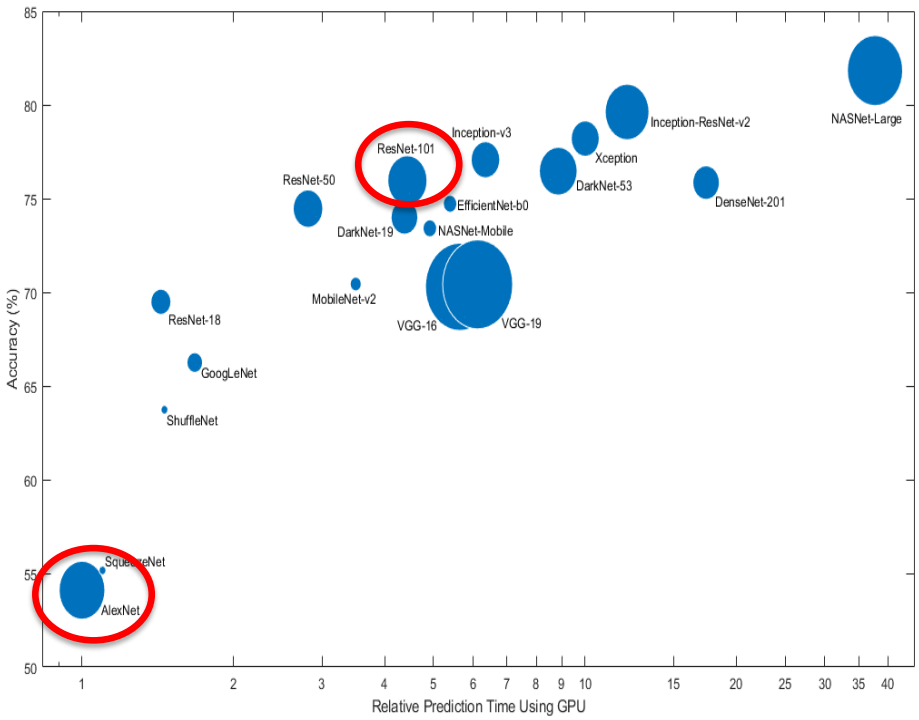

Figure 4: Comparison of accuracy and runtime for neural networks [8].

To train and evaluate a neural network, the data is divided into three data sets: one for training, one for validation, and one for testing. The training and validation data sets are used when the network is trained. A convolutional neural network works by convolving a window over an image and using the regions from the window as input to the neural network. Neural networks have an input layer, output layer, and hidden layers, as shown in Figure 5. Each of the layers has one or more nodes, or neurons, that has a weight associated with it [9].

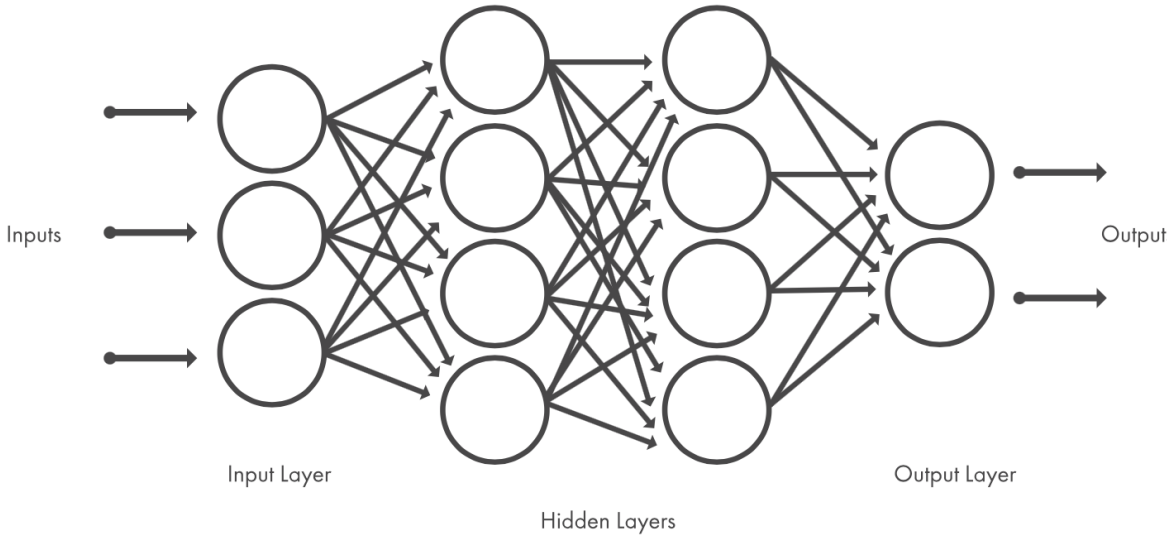

Figure 5: An example diagram of a neural network [9].

The training data is processed by the network and the network's weights are updated using backpropagation if the footprint is misclassified. After a user-defined number of iterations, the validation data is given to the network, and it determines the classes for each footprint. In the validation phase, which occurs periodically in the training phase, the network weights are not updated, even if the footprints are misclassified. This

means that the validation data is never used to train the neural network; it only serves to evaluate the performance of the neural network training.

Once the neural network is trained, it is used on the testing data set to assess its performance on unseen data. This step is used to assess the accuracy of the neural network to classify unknown data. This helps to determine if the neural network and transfer learning can be used to classify SMAP RFI sources. After neural networks are trained and their parameters are finely tuned, they are evaluated using a confusion matrix. A confusion matrix is an analysis tool used in machine learning to show the number of true positives, true negatives, false positives, and false negatives for a neural network. The bottom row shows recall and the rightmost column displays precision [10].

Data preparation.

The first test was performed to demonstrate the concept of using transfer learning to classify the SMAP footprints into the previously defined categories (no RFI, narrowband RFI, and wideband RFI). For this initial experiment, a small data set was gathered, and the footprints were sorted by hand. Both AlexNet and Resnet-101 were trained and tested on this first attempt. A total of 1,012 SMAP footprints were divided into each class: 400

CLASS	NUMBER OF FOOTPRINTS
NO RFI	400 (279 training, 12 validation, 109 testing)
NARROWBAND	400 (279 training, 12 validation, 109 testing)
WIDEBAND	312 (218 training, 9 validation, 85 testing)

Table 1: The number of hand sorted footprints, restricted to have approximately the same number in each class.

spectrograms were labeled as containing no RFI, 400 spectrograms were labeled as containing narrowband RFI, and 312 spectrograms were labeled as containing wideband RFI. To prevent the neural network from overtraining on one class, the number of SMAP footprints in each class is of the same order of magnitude, as shown in Table 1.

Results

Both AlexNet and Resnet-101 were trained using the same parameters, with the validation images being tested every 129 iterations during the training phase. The confusion matrices of each neural network are shown in Figure 6. They present the accuracy of the neural network to classify the footprints of the testing data set (i.e., the unknown data).

Figure 6: The confusion matrices for the test data using both AlexNet (left) and Resnet-101 (right).

Both networks present an overall high accuracy of 97.7% and 98.3% for AlexNet and ResNet-101, respectively. Despite the small number of footprints in each class, these seem to confirm our hypothesis that deep learning can be used to classify the footprints based on RFI type. However, this initial data set was very limited, due to the hand-sorting of the footprints. Therefore, it was necessary to develop an automated way to create a larger dataset. Doing so will allow for more examples of each type of RFI to be used in training the network, making the neural network more robust.

RFI Type Classification Further Testing

Materials and Methods

Hand sorting the data produced a limited number of footprints, so a way to automate the sorting of footprints was created. In this study, the classification of the spectrograms now relies on one of the SMAP RFI algorithms, the cross-frequency algorithm, that looks for rapid changes of the brightness temperature across the frequency channels. This algorithm flags the frequency channels that contain RFI.

The classification of the spectrograms is based on the following conditions:

- If no frequency channels are flagged by the cross frequency algorithms and by any other SMAP RFI detection algorithms, then the spectrogram was sorted into the no RFI class.
- If the number of frequency channels flagged by the cross frequency algorithms was between one and five (inclusive), the spectrogram was classified as containing narrowband RFI.
- If the number of frequency channels flagged by the cross frequency algorithm was greater than 5, then further processing was performed to determine if the spectrogram contained wideband RFI, multiple cases of narrowband RFI, or a more complicated RFI case.

In the last case, the classification is based on the number of consecutive frequency channels flagged by the cross frequency algorithm:

- If five or more channels were consecutively flagged, the footprint was labelled as containing wideband RFI.
- If the number of consecutive channels flagged was less than five each time, then it was marked as having repeated cases of narrowband RFI sources.

Figure 7 presents an example of the labelling of three SMAP spectrograms using the cross frequency algorithm. These footprints are classified as containing narrowband RFI (left), wideband RFI (middle) and two narrowband RFI (right). The initial labelling of the footprints is crucial, as the network needs to train on accurate data set in order to avoid misclassification. It is important to present all the possible examples of spectrograms contaminated by RFI to the neural network so that the training is the most inclusive possible. The total number of footprints in each class are shown in Table 2.

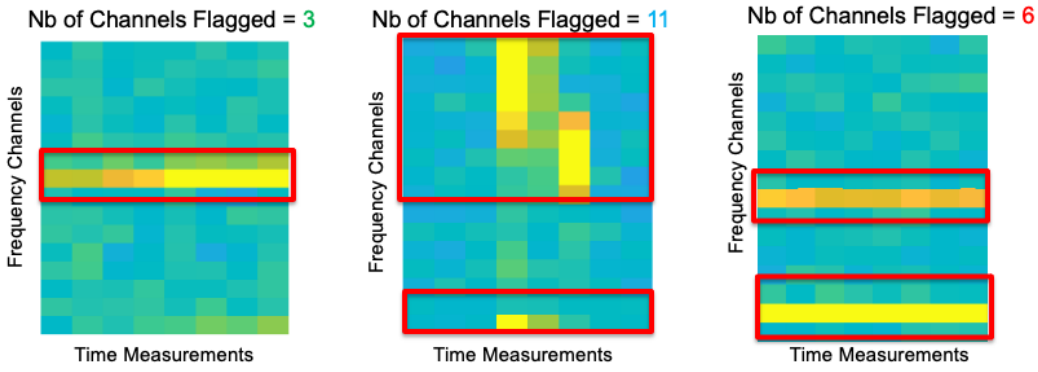

Figure 7: Example of the labelling of SMAP spectrograms using the cross frequency algorithm. The footprint on the left is labelled as containing narrowband RFI, the footprint in the middle as containing wideband RFI and the last footprint as containing two narrowband RFI. The red rectangle highlights the frequency channels flagged by the cross frequency algorithm.

FOLDER	CLASS	NUMBER OF FREQUENCY CHANNELS FLAGGED	RFI	NUMBER OF FOOTPRINTS
No RFI	no RFI	0	0	23,052
Multiple cases of narrowband	narrowband	Greater than 5	assorted	83,547
One case of narrowband	narrowband	Greater than 0, Less than or equal to 5	assorted	385,497
Wideband	wideband	Greater than 5	assorted	144,664

Table 2: The number of automatically sorted footprints.

Given that AlexNet is faster to train, this part of the study focuses on the training and testing of AlexNet on this new generated data set. Two experiments were run. The first one was initiated to assess the effect of reducing the number of footprints to be similar between classes, which would prevent over-training. The second experiment was performed to test the difference between the two narrowband classes (multiple vs one case of narrowband RFI).

Results

To demonstrate the importance of distinguishing between the "wideband RFI" class and the "multiple narrowband RFI" class when the number of frequency channels flagged is greater than five, a simple test was performed. The neural network AlexNet was trained on three classes only: no RFI, one narrowband RFI class, and wideband class. The results of the testing of the network are presented in Figure 8. In this test, it is observed that AlexNet mostly misclassifies wideband RFI as narrowband RFI, as the wideband class has a lower recall value than for the other two classes. Even though the number of frequency channels flagged by the cross frequency algorithm is greater than 5, this spectrogram contains two narrowband RFI sources. This confirms the necessity of dividing this class into wideband RFI and multiple narrowband RFI.

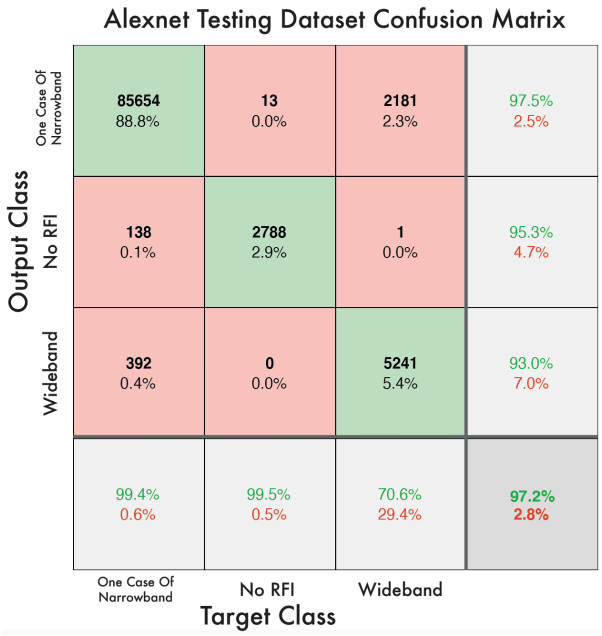

Figure 8: The confusion matrix when AlexNet was trained on three classes: no RFI, one case of narrowband, and wideband classes.

The second experiment aims at assessing the performance of AlexNet when the neural network is trained on a restricted number of footprints (20,000) per class. In this test, the classes were limited to one instance of narrowband RFI (i.e., the number of frequency channels flagged less than 5), wideband RFI, and no RFI. The results of the testing of AlexNet on unknown data set for that experiment is presented in Figure 9.

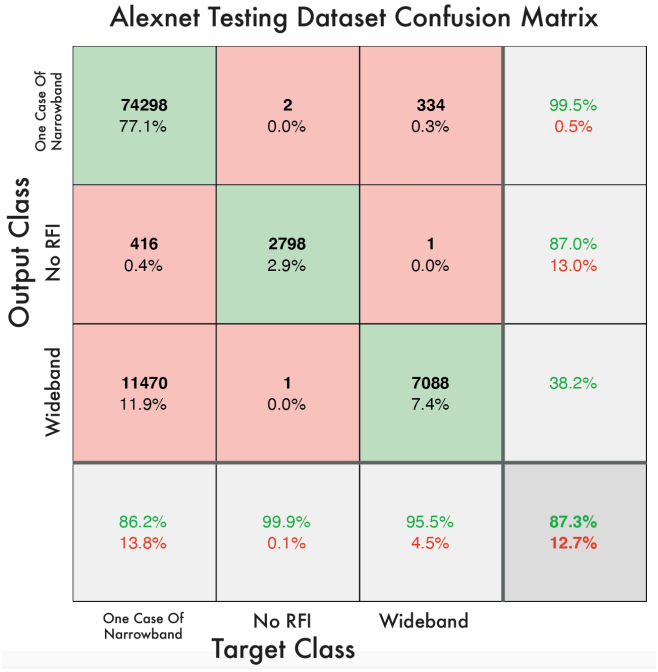

Figure 9: The confusion matrix when AlexNet was trained on restricted number of footprints for one case of narrowband, no RFI, and wideband classes.

For this particular experiment, the wideband class's precision is much lower than the other two classes. The confusion matrix shows that many footprints containing one narrowband RFI are misclassified as footprints containing wideband RFI. Since the overall accuracy of the classification is 10% lower than the previous test, it seems that training the neural network on a restricted number of footprints, so that all the classes have approximately the same number of footprints, induces more misclassifications. A plausible

explanation for these results is that limiting the number of footprints provided fewer training examples for narrowband RFI and wideband RFI, so they were more often misclassified as each other.

The last experiment consisted in training AlexNet on all the possible examples of RFI. This means that the narrowband RFI class includes footprints with fewer than five frequency channels flagged, as well as footprints containing multiple instances of narrowband RFI (which means the number of frequency channels flagged is greater than five). The confusion matrix of the testing of AlexNet trained over all the classes is presented in Figure 10. It is observed that the neural network misclassifies footprints labeled with wideband RFI the most, as the precision and recall is the lowest for the wideband class.

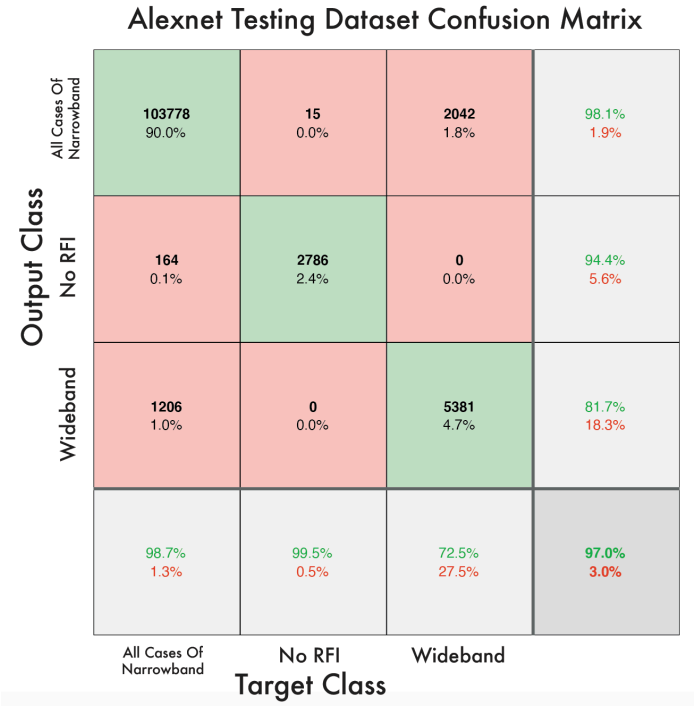

Figure 10: The confusion matrices when AlexNet was trained on all narrowband, no RFI, and wideband classes.

From the results of the different tests performed, it can be concluded that, while the neural network is capable of learning the classification, it particularly struggles to classify footprints containing wideband RFI. The results also demonstrate that the network trains as well when only footprints containing one case of narrowband RFI are included as when footprints containing all cases of narrowband are considered. This is confirmed by the misclassification error of the footprints containing narrowband RFI being less than 1% in both cases.

Training on an equal number of footprints for each class did not increase the overall accuracy of the network. This might be explained by the restricted number of footprints. Further testing would need to be performed to confirm this hypothesis.

Training on all the narrowband footprints, instead of a subset, shifted the misclassified footprints from mostly narrowband being misclassified as wideband to a mix of narrowband and wideband being misclassified as each other.

The results from the initial testing were presented at the RFI workshop 2021 [11].

Materials and Methods

Despite the implementation of algorithms for RFI detection and filtering, RFI is still frequently noticeable in SMAP data. The second part of this study focuses on investigating the use of basic image processing techniques to detect residual RFI in weekly max hold maps of SMAP antenna temperature after RFI detection is applied. The goal of this study is to understand if image processing algorithms (that could be developed into machine learning algorithms) could help identify areas that are impacted by residual RFI.

Before investigating the use of machine learning algorithms, this initial analysis implemented a mean filter to look for significant spatial variations in the max hold maps of the filtered antenna temperature. The mean filter is a basic filter used in image processing where the value for each pixel is found by averaging its value with its 8 neighbor pixels. An example of a mean filter is shown in Figure 11.

1/9	1/9	1/9
1/9	1/9	1/9
1/9	1/9	1/9

Figure 11: An example of an n by n mean filter, where n=3.

The input to the algorithm is the weekly max hold maps of the antenna temperature after RFI detection and filtering were applied. The filter convolves over the global map and flags pixels that present a significant difference from its surrounding pixels. These flagged pixels will most likely be pixels containing residual RFI. An example of how the filter convolves around the input map is shown in Figure 12.

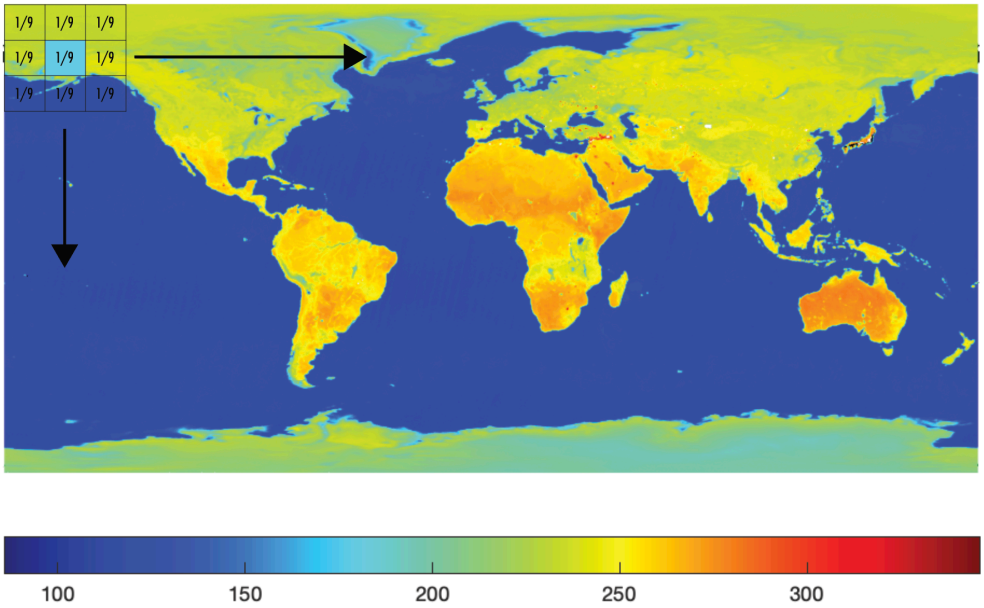

Figure 12: This shows an example of a (not to scale) filter and how it convolves, first moving across the row to the right, then resetting itself on the left edge, one row down.

The first step of this work is to mask the ocean and the inland water to avoid detecting coastlines or shores, as they present a significant transition between the colder antenna temperature acquired over water and the warmer antenna temperature measured over land. The mean filter is then applied on the weekly max hold maps of the filtered antenna temperature over the 8 years of SMAP mission. For each week, areas impacted by

residual RFI are identified. In this study, the impact of the size of the mean filter is assessed, as well as the detecting threshold.

Results

The first analysis explores the effect of the filter size on the detection of residual RFI. Figure 13 presents the results of the detection using a mean filter of size 3x3 (Figure 13b), 11 x 11 (Figure 13c) and 19 x 19 (Figure 13d) and is an example of the original max hold map of the filtered antenna temperature over the middle east. On this figure, residual RFI can clearly be identified on the Mediterranean coast and in Saudi Arabia. From the comparison in Figure 13, it can be observed that smaller filters are more suitable to detect smaller patches of residual RFI, whereas using a larger filter helps filtering residual RFI covering a larger area.

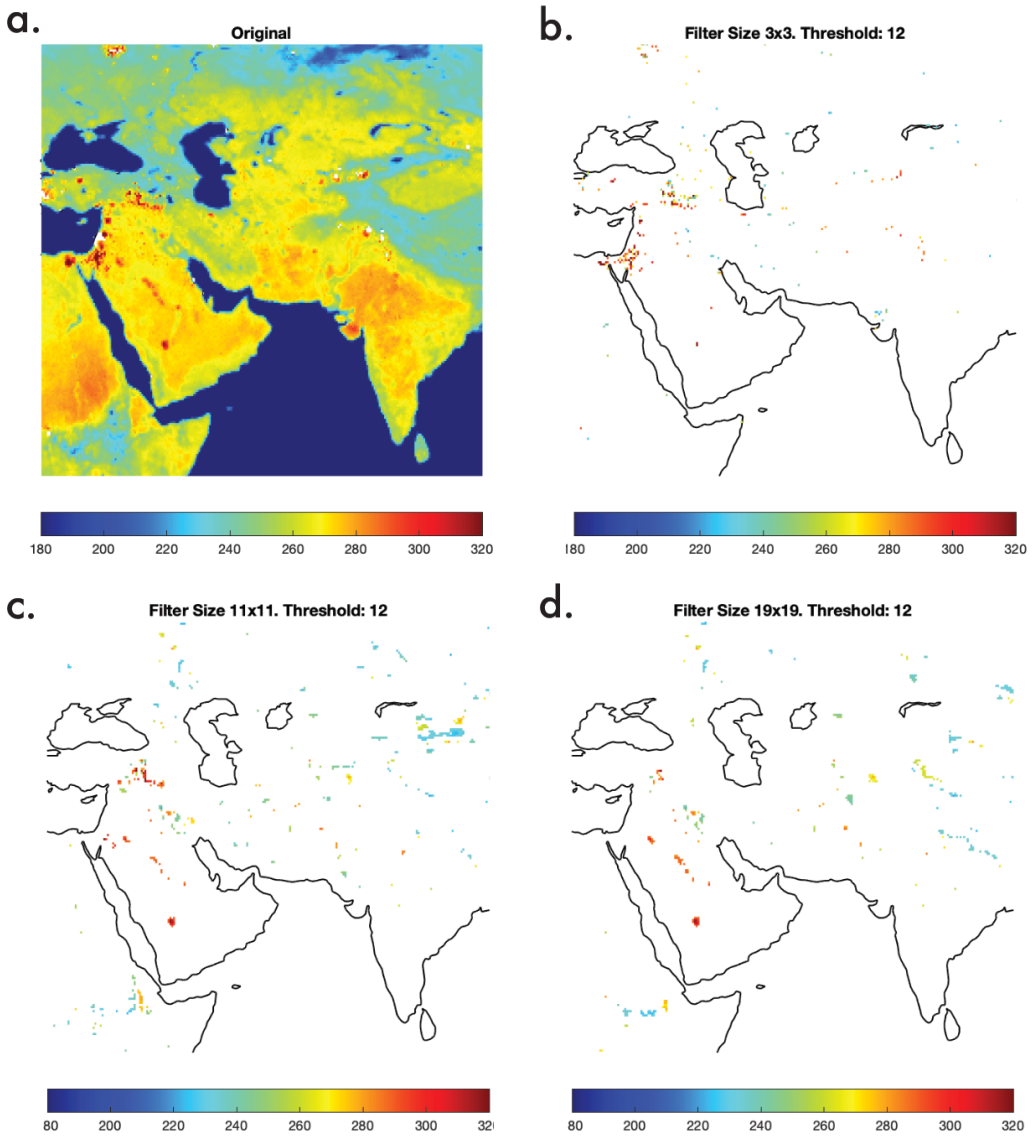

Figure 13: These images show the effect that different filter sizes have on the ability of the filter to flag residual RFI. Part a shows the original map before any filtering. This results when filter sizes of 3x3, 11x11, and 19x19 are shown in parts b, c, and d, respectively.

The effect of the threshold of the mean filter on the detection of residual RFI was also explored, and the results are shown in Figure 14.

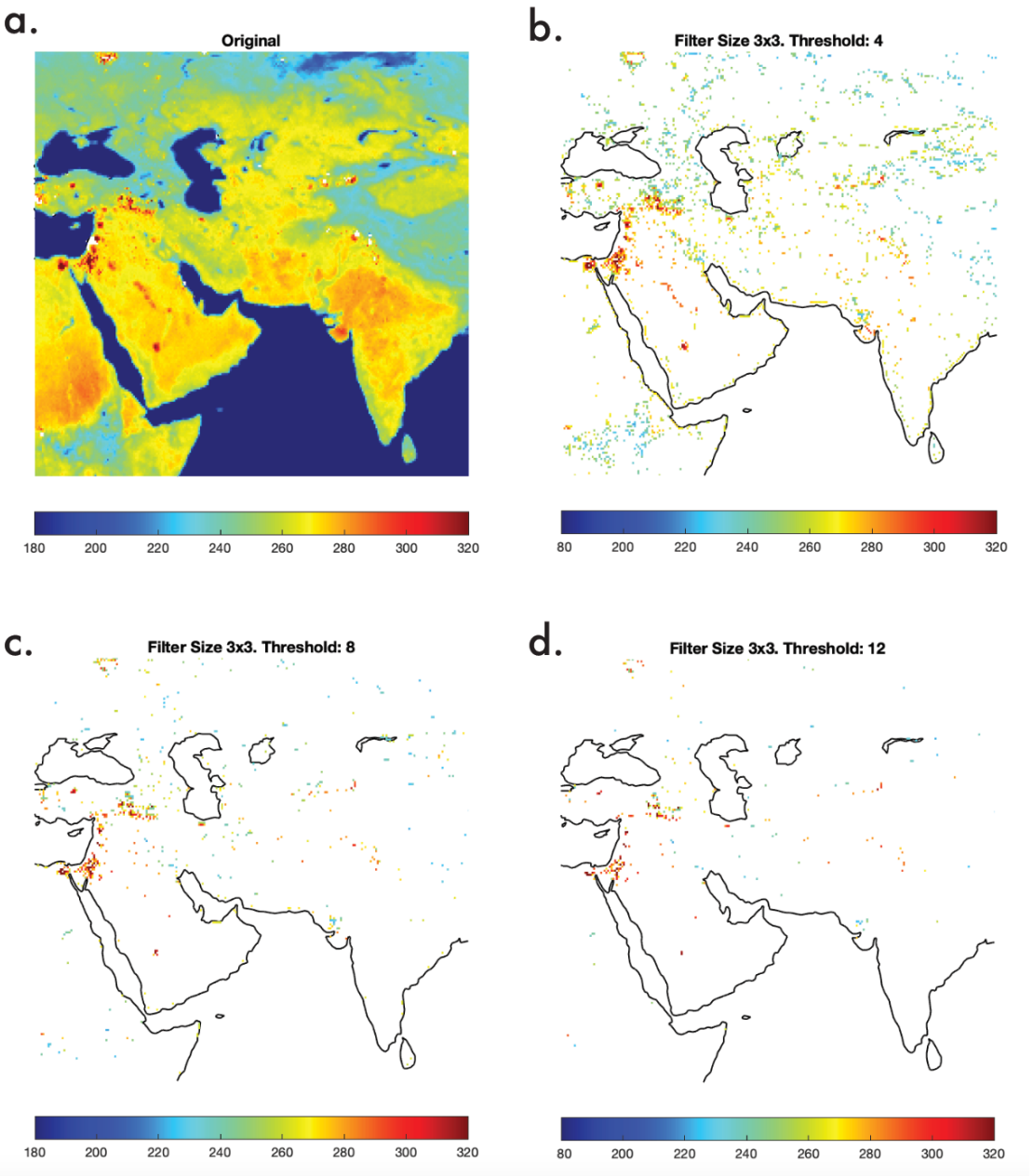

Figure 14: The effect that the threshold has on the output. Part a shows the original map before any filtering. The results when thresholds of 4, 8, and 12 are shown in parts b, c, and d, respectively.

When the threshold value is low, as in part b, a lot of non- residual RFI pixels are flagged inducing a high false alarm rate. Increasing the threshold to a moderate threshold results in lower false alarm rate as less non residual RFI pixels are flagged. A stricter threshold, shown in part d, has a very low false alarm rate, but also a higher misdetection rate, as some residual RFI remain undetected in this case. The misdetections are because, in the case of larger areas impacted by residual RFI, the difference between the mean value of the surrounding pixels and the contaminated pixels will not be large enough to be identified as residual RFI, which results in a misdetection.

The initial results for the mean filtering algorithm show that it could accurately detect a variety of areas impacted by residual RFI in the max hold maps of the filtered antenna temperatures. However, in order to build a robust algorithm to detect all residual RFI, different filter sizes and thresholds will have to be considered depending on the location of the residual RFI sources and the size of the area impacted. This indicates the potential of using a machine learning algorithm that could optimize the size of the filter and/or the threshold to improve the detection of residual RFI.

Conclusions and Future Recommendations

This work was divided into two parts. The first one aims at using machine learning algorithms to classify RFI sources to provide information about the RFI type. The second part of the project focused on detecting residual RFI in the SMAP max hold maps of the antenna temperature, after RFI detection is applied, using basic image processing techniques.

Being able to classify the RFI type is important for many reasons. The first is that, after the RFI type is detected, we can adapt existing algorithms to better detect and filter the RFI. Additionally, knowing where the RFI is occurring on the globe will give us more information about the global RFI environment.

Our results support both concepts that RFI can be classified using neural networks, along with that residual RFI can be detected using mean filtering. Although some classes of RFI footprints were still being misclassified, in many of our tests, the neural networks had a testing accuracy around 97%.

One of the biggest limiters to the RFI type classification was the amount of time needed to generate and process a large number of the footprints. Another time-related limiter was the significant training time of the neural networks. By focusing on limiting the training time, we were able to demonstrate that it was successful at a smaller scale. More computing power, which would enable us to train the networks more thoroughly,

would further improve the results. Having more examples of narrowband and wideband footprints, along with training the networks for longer, should decrease the misclassification between narrowband and wideband footprints.

We also demonstrated that mean filtering provides encouraging initial results for detecting residual RFI in the max hold maps of the SMAP filtered antenna temperature. Because the size of the filter and threshold for filtering vary based on the area impacted by the residual RFI, the algorithm should further be developed. A machine learning model would be used to train on and adapt the size and threshold of the filter depending on the size of the RFI patch to identify areas impacted by residual RFI, since the residual RFI can impact areas of different sizes.

Bibliography

[1] NASA. (2020, February 4). *Specifications*. NASA. Retrieved October 15, 2021, from https://smap.jpl.nasa.gov/observatory.

[2] Piepmeier, J. R., Johnson, J. T., Mohammed, P. N., Bradley, D., Ruf, C., Aksoy, M., Garcia, R., Hudson, D., Miles, L., & Wong, M. (2014). Radio-frequency interference mitigation for the Soil Moisture Active Passive Microwave Radiometer. *IEEE Transactions on Geoscience and Remote Sensing*, *52*(1), 761–775. https://doi.org/10.1109/tgrs.2013.2281266.

[3] Bringer, A., Johnson, J. T., Soldo, Y., Le Vine, D. M., Mohammed, P., Misra, S., de Matthaeis, P., & Piepmeier, J. R. (2021b). Properties of the RFI environment at 1400–1427 MHz as observed by the soil moisture active/passive mission microwave radiometer. *IEEE Journal of Selected Topics in Applied Earth Observations and Remote Sensing*, *14*, 7259–7267. https://doi.org/10.1109/jstars.2021.3092996.

[4] Mohammed, P. N., & Piepmeier, J. R. (2021). Microwave radiometer RFI detection using deep learning. *IEEE Journal of Selected Topics in Applied Earth Observations and Remote Sensing*, *14*, 6398–6405. https://doi.org/10.1109/jstars.2021.3091873.

[5] Bringer, A., Johnson, J.T., Mohammed, P.N. and Piepmeier, J.R., 2017, July. Performance of SMAP radiometer RFI detection algorithms and analysis of residual RFI sources. In *2017 IEEE International Geoscience and Remote Sensing Symposium (IGARSS)* (pp. 1243-1246). IEEE.

[6] Soldo, Y., Le Vine, D. and de Matthaeis, P., 2019. Detection of residual "Hot Spots" in RFI-filtered SMAP data. *Remote Sensing*, *11*(24), p.2935.

[7] *Get Started with Transfer Learning*. MATLAB & Simulink. (n.d.). Retrieved from https://www.mathworks.com/help/deeplearning/gs/get-started-with-transfer-learning.html.

[8] *Transfer Learning*. MATLAB & Simulink. (n.d.). Retrieved from https://www.mathworks.com/discovery/transfer-learning.html.

[9] *What is a neural network?* What Is a Neural Network? - MATLAB & Simulink. (n.d.). Retrieved March 27, 2023, from https://www.mathworks.com/discovery/neural-network.html.

[10] *confusionchart*. Create confusion matrix chart for classification problem MATLAB.(n.d.). Retrieved March 27, 2023, from https://www.mathworks.com/help/stats/confusionchart.html.

[11] Bringer, A., Bete, A., Johnson, J. T., Mohammed, P., & Misra, S. R. (2021). Using Machine Learning Algorithms to Detect and Classify RFI: Illustration Using Soil Moisture Active/Passive (SMAP) Data.